X-Ray Computed Tomography to Measure Bed Density in Sand Transport

Corinne Brunelle, Pierre Francus, Benoît Camenen, Carl L Amos, Mathieu Des Roches, Emeline Perret, Hachem Kassem, Louis-Frédéric Daigle, Philippe Després

▶ **To cite this version:**

Corinne Brunelle, Pierre Francus, Benoît Camenen, Carl L Amos, Mathieu Des Roches, et al.. X-Ray Computed Tomography to Measure Bed Density in Sand Transport. Journal of Hydraulic Engineering, 2022, 148, ⟨10.1061/(asce)hy.1943-7900.0002025⟩. ⟨hal-03948247⟩

HAL Id: hal-03948247

https://hal.inrae.fr/hal-03948247v1

Submitted on 20 Jan 2023

HAL is a multi-disciplinary open access archive for the deposit and dissemination of scientific research documents, whether they are published or not. The documents may come from teaching and research institutions in France or abroad, or from public or private research centers.

L'archive ouverte pluridisciplinaire **HAL**, est destinée au dépôt et à la diffusion de documents scientifiques de niveau recherche, publiés ou non, émanant des établissements d'enseignement et de recherche français ou étrangers, des laboratoires publics ou privés.

HAL Authorization

Technical Note

X-Ray Computed Tomography to Measure Bed Density in Sand Transport

Corinne Brunelle, Ph.D.[1]; Pierre Francus[2]; Benoît Camenen[3]; Carl L. Amos[4]; Mathieu Des Roches[5]; Emeline Perret[6]; Hachem Kassem[7]; Louis-Frédéric Daigle[8]; and Philippe Després[9]

Abstract: This paper reports a new experimental method applying medical X-ray computed tomography (CT) to estimate the bed load in sand transport. A set of current-generated sand ripple experiments were conducted in a small hydraulic flume inserted in the CT scanner. The methodology is based on the measurements of height, velocity, and density of bed forms to estimate bed load. A temporal series of bed topography is first extracted from the CT scan images. The velocity is estimated by tracking the displacement of bed forms from two successive bed topographies. The sand bed density (ρ_{sb}) is estimated from the CT scan measurements using a calibration technique. The method measuring ρ_{sb} to calculate bed load is validated comparing measurements made with sand traps. The advantages and limitations of the CT method applied to bed-load transport are discussed. **DOI: 10.1061/(ASCE)HY.1943-7900.0002025.** *© 2022 American Society of Civil Engineers.*

Practical Applications: Sediment transport is a fundamental physical process in Earth Sciences. It refers to the movement of sediment grains transported by water currents and deposited where or when water flow ends. This cycle seems at first inoffensive but could impact millions of human lives all around the world. River floods, sea-level rise, and storms are likely to modify the landscape of many populated areas located nearby in the next decades. A better understanding of sediment transport processes would greatly benefit our capacity to determine the impact of those extreme events on river and coastal morphology. To achieve this, physical models are used in laboratories to simulate sediment dynamics at a smaller scale. These results help researchers developing numerical models of sediment transport to better predict river dynamics as well as the movement of coastlines. This study is an insight on the application of new laboratory techniques using advanced three-dimensional imaging technique as an effort to contribute to our knowledge of sediment dynamics.

Introduction

Bed-load transport—the transport rate of unsuspended grain by flowing water—of fine sediments is often observed through bed form migration. However, bed-load transport remains difficult to measure and quantify using laboratory and field techniques. Sediment traps are generally used (Roberts et al. 2003; Holmes 2010; Mrokowska et al. 2018; Khosravi et al. 2019), but they only provide a local section-averaged and temporally averaged estimation of bed-load transport. Yet, most of the classical equations (Khorram and Ergil 2011) for bed-load transport are derived from this averaged trap method. Acoustic tools such as the acoustic Doppler velocity profiler (ADVP) (Blanckaert et al. 2017) or acoustic concentration and velocity profiler (ACVP) (Hurther et al. 2011) can be used to evaluate bed-load characteristics, but for a single point only. Bed-load transport can also be estimated using the mass conservation equation, known as the Exner equation, by calculating the bed-form velocity (McElroy and Mohrig 2009); this method is commonly known as the dune-tracking method. It can be nonintrusively established by acquiring a temporal series of bed topography and tracking the displacement of the bed forms with time (Muste et al. 2016; Tsubaki et al. 2018). However, there is still one parameter of the Exner equation that is roughly approximated, which is the dry sand bed density (ρ_{sb}). The density of a sand layer including

[1]Physical Scientist, Ocean Science Branch, Fisheries and Oceans Canada, 2121 Transcanadienne, Dorval, QC, Canada H9P 1J3 (corresponding author). ORCID: https://orcid.org/0000-0002-9326-4712. Email: corinne.bourgault-brunelle@dfo-mpo.gc.ca

[2]Professor, Canada Research Chair in Environmental Sedimentology, Institut National de la Recherche Scientifique, Centre Eau Terre Environnement, 490 Couronne St., QC, Canada G1K 9A9. Email: pierre.francus@inrs.ca

[3]Researcher, Institut national de recherche pour l'agriculture, l'alimentation et l'environnement (INRAE), UR RiverLy, CS 20244, 5 Doua St., Villeurbanne 69625, France. Email: benoit.camenen@inrae.fr

[4]Emeritus Professor, National Oceanography Centre, Univ. of Southampton, Ocean and Earth Science, University Rd., Highfield, Southampton SO17 1BJ, UK. Email: carllamos@gmail.com

Note. This manuscript was submitted on December 28, 2021; approved on July 19, 2022; published online on October 6, 2022. Discussion period open until March 6, 2023; separate discussions must be submitted for individual papers. This technical note is part of the ***Journal of Hydraulic Engineering***, © ASCE, ISSN 0733-9429.

[5]Research Assistant, Multidisciplinary Laboratory for Non-Medical Use, Institut National de la Recherche Scientifique, Centre Eau Terre Environnement, 490 Couronne St., QC, Canada G1K 9A9. ORCID: https://orcid.org/0000-0002-2729-2715. Email: mathieu.des_roches@inrs.ca

[6]Research Engineer, Institut National de Recherche Pour l'Agriculture, l'Alimentation et l'Environnement (INRAE), UR RiverLy, CS 20244, 5 Doua St., Villeurbanne 69625, France. ORCID: https://orcid.org/0000-0002-4444-6640. Email: e.perret@cnr.tm.fr

[7]Teaching and Research Fellow, National Oceanography Centre, Univ. of Southampton, Ocean and Earth Science, University Rd., Highfield, Southampton SO17 1BJ, UK. ORCID: https://orcid.org/0000-0002-5936-6037. Email: hachem.kassem@soton.ac.uk

[8]Technical Assistant, Multidisciplinary Laboratory for Non-Medical Use, Institut National de la Recherche Scientifique, Centre Eau Terre, Environnement, 490 Couronne St., QC, Canada G1K 9A9. Email: louis-frederic.daigle@inrs.ca

[9]Professor, Département de physique, de génie physique et d'optique, Faculté des sciences et de génie, Université Laval, 2325 Université St., QC, Canada G1V 0A6. ORCID: https://orcid.org/0000-0002-4163-7353. Email: philippe.despres@phy.ulaval.ca

Downloaded from ascelibrary.org by INRAE on 12/06/22. Copyright ASCE. For personal use only; all rights reserved.

voids is indeed difficult to measure in real time without disturbing the experiments or the bed structures. Recent studies attempted estimating sediment matter density in water flows in a nonintrusive way for multiphase flows using Synchrotron X-ray (Kastengren and Powell 2014) and gamma-ray attenuation. However, these approaches are restricted to very small volumes (Mayar et al. 2020).

This technical note explores the use of medical X-ray computed tomography (CT) to estimate ρ_{sb} in the bed-load layer. CT is a nondestructive technique applied in numerous fields of geosciences to calculate a three-dimensional attenuation coeffcient matrix of the scanned object scaled in Hounsfield units (HU), which is physically related to matter density (Ketcham and Carlson 2001; Otani and Obara 2004; Ketcham and Iturrino 2005). The large opening of medical CT scanners allows for a small hydraulic flume to be installed within the scanner's gantry. Previous studies have shown promising results in quantifying sediment transport processes using this kind of setting (Yamada et al. 2013; Tilston et al. 2015; Brunelle 2019). However, it has not been demonstrated how precise and accurate the medical CT scanner is when deriving the bed-load transport, especially for moving sand grains with particle size (D) smaller or close to the CT image resolution (0.56 mm). In this case, any segmentation technique that classifies CT image pixels to differentiate the volume of sand and void (Griffin et al. 2012) is not applicable. CT also suffers from numerous image artifacts (Hsieh 2009) that might compromise its application when using large and squared objects such as a uniform and rectangular hydraulic flumes filled with a movable sand bed.

To estimate the potential of medical CT scanner for the study of fine and noncohesive sediment bed-load transport in the laboratory, a series of flume experiments over a mobile sand bed with increasing unidirectional flow velocities is performed. First, the data analysis procedure is detailed in order to extract the parameters of the bed-load transport equation (i.e., bed shear stress, bed elevation, bed-form velocity, and bed density) from measurements (i.e., water velocity and HU). Secondly, the resulting bed-load rates are compared to sand trap measurements carried out at the downstream end of the flume. Based on the experimental results, the manuscript discusses the potentialities and limitations of the method.

Method

In the following sections, spatial averages are indicated with angled bracket symbols ($< >$), with averaged dimensions in subscript and time averages with the overbar symbol ($\bar{}$). The indices x, y, and z indicate the averaged dimensions along the x, y, z-directions. The x, y, z-axes are oriented streamwise, transversely, and vertically, respectively. The sand bed load (q_{sb}), in terms of mass flow rate per unit width (kg m^{-1} s^{-1}), is computed as

$$q_{sb} = \rho_{sb} V \eta \tag{1a}$$

where ρ_{sb} is the dry sand bed density; V is the mass flow velocity, here estimated from the bed-form velocity; and η is the sand bed elevation. The error (ε) on bed load is estimated by using the propagation of error method from the right-hand side of Eq. (1a) as described by Bevington and Robinson (2003) for multiplicative terms

$$\varepsilon_{q_{sb}} = q_{sb}\sqrt{\left(\frac{\varepsilon_{\rho_{sb}}}{\rho_{sb}}\right)^2 + \left(\frac{\varepsilon_V}{V}\right)^2 + \left(\frac{\varepsilon_\eta}{\eta}\right)^2} \tag{1b}$$

The dry sand bed density ρ_{sb} is computed using the CT scanner measured values in HU. The HU values vary from $-1{,}024$ to $+3{,}071$, providing 4,096 levels relative to matter density. A voxel of the CT scan image contains a percentage of water and sand. The CT measurement of the wet sand bed (HU_{sb}) is therefore converted into dry sand bed density by testing the following expression:

$$\rho_{sb} = \rho_s \frac{(HU_{sb} - HU_w)}{(HU_q - HU_w)} \tag{2}$$

where ρ_{sb} is a function of the CT scan measurement of water (HU_w), quartz (HU_q), and the density of the sand grain (ρ_s), which is uniform and equal to pure quartz ($\rho_s = \rho_{quartz}$). A 2-cm^3 piece of pure quartz mineral is buried in the sand bed to determine the reference value of HU_q. The sand bed density ρ_{sb} is not considered to be time- or space-dependent, and the precision of using the three-dimensional spatial average of dry sand bed density $[<\rho_{sb}(x, y, z)>_{xyz}]$ as an input for Eq. (1) is evaluated.

The bed-form velocity and bed elevation are time- and space-dependent. Consequently, these parameters are both estimated in space (xy) but for a period or an instantaneous time, respectively. The cross-correlation algorithm developed by Scarano (2012), using LaVision software, calculates the temporal average of bed-form velocity vector field ($\bar{V}$) from two successive 2D bed elevation maps separated by a time interval T (Table 1). The calculation creates a 2D vector grid (x, y) of bed-form velocities. Only the temporal average of bed-form velocity in the streamwise direction ($\bar{V}_x$) is kept for Eq. (1) representing the solid transport in the flow direction. The missing velocity values, where the cross-correlation algorithm failed to calculate velocity, were estimated by calculating the average to closest neighbors.

The bed elevation η is extracted from the 3D HU matrix measured by CT scan to obtain the sand bed topography. In this study, the level $\eta = 0$ is chosen as the minimum of the bed topography. A threshold value of $\mathrm{HU} = 400$ is used to distinguish water and sand, considering that water and sand HU values are significantly different (where $\mathrm{HU} > 400$ corresponds to sand); HU_w values are around 0. Only the second measurement of bed topography is used in Eq. (1) to specify η, neglecting the change in shape of bed forms with time during measurements as a result of technical limitations.

The velocity $[\bar{V}_x(x, y)]$ and height $[\eta(x, y)]$ of bed forms are discretized on the bed topography xy-grid. Eq. (1) returns the time-averaged bed load in the xy-plane $[\bar{q}_{sb}(x, y)]$. The bed load is expressed as a function of fluid bed-shear stress τ_0. The bed-shear stress is estimated by the quadratic stress law

Table 1. Experimental conditions for sand bed experiments (EXP)

Experiment	$\bar{Q}$ (m^3 s^{-1})	d (m)	$\bar{U}$ (m s^{-1})	Fr	Re	$\bar{\theta}$	L (m)	T (s)	$<\bar{V}_x>_{xy}$ (mm s^{-1})	$<\rho_{sb}>_{xyz}$ (kg m^{-3})	$<\bar{q}_{sb}>_{xy}$ (kg m^{-1} s^{-1})
EXP1	0.008	0.140	0.19	0.16	4,433	0.029	1.20	810	0.016 (0.002)	1,060 (186)	0.00014 (0.00003)
EXP2	0.010	0.140	0.24	0.20	5,600	0.047	0.30	200	0.10 (0.03)	1,060 (186)	0.0025 (0.0005)
EXP3	0.012	0.140	0.29	0.25	6,766	0.068	0.20	80	0.18 (0.08)	1,087 (212)	0.0053 (0.0012)
EXP4	0.012	0.120	0.33	0.30	6,600	0.092	0.10	30	0.56 (0.06)	1,113 (159)	0.013 (0.002)

Note: Water discharge ($\bar{Q}$) initial water depth (d), section and time averaged fluid velocity ($\bar{U}$) estimated using ($\bar{Q}$), Reynolds (Re) and Froude (Fr) numbers using $\bar{U}$, Shields' parameter ($\bar{\theta}$). The standard deviations of mean values are in parentheses. The time- and space-averaged bed-form velocity, indicated by overbars and subscripts, respectively, in the x-direction ($<\bar{V}_x>_{xy}$) and bed-load transport $<\bar{q}_{sb}>_{xy}$, and space-averaged sand bed density in the bed-load layer ($<\rho_{sb}>_{xyz}$) are listed. The length (L) and time between CT scans (T) are indicated.

Downloaded from ascelibrary.org by INRAE on 12/06/22. Copyright ASCE. For personal use only; all rights reserved.

$$\overline{\tau_0} = \rho C_d \bar{U}^2 \tag{3}$$

where $\bar{U}$ is the mean flow velocity and ρ is the water density. The mean flow velocity $\bar{U}$ is expressed as a function of the time-averaged water discharge ($\bar{Q}$), the width of the flume (W), and the initial water depth over flat bed (d), $\bar{U} = \bar{Q}/Wd$, where $W = 0.30$ m. The empirical nondimensional drag coefficient C_d depends on the vertical flow velocity profile and is evaluated assuming a logarithmic profile (Soulsby 1983):

$$C_d = \left(\frac{\kappa}{1 + \ln(\frac{z_0}{d})}\right)^2 \tag{4}$$

where κ is von Karman's constant ($\kappa = 0.41$); and z_0 is the hydraulic roughness length. z_0 is associated with the apparent bed roughness (k_s), commonly called equivalent sand roughness, quantified as $k_s = 30z_0$ (Nikuradse 1933). The bed roughness is expressed as a function of grain size, $k_s = 2D_{90}$ (Yalin 1972), where D_{90} is the 90th percentile of grain-size distribution. The bed-shear stress is described in terms of a nondimensional bed-shear stress, commonly named the Shields' parameter (θ) after Shields (1936)

$$\bar{\theta} = \frac{\overline{\tau_0}}{(\rho_s - \rho)gD_{50}} \tag{5}$$

where D_{50} is the 50th percentile of grain-size distribution and g is the acceleration of gravity (9.81 m s^{-2}). The results are compared to the bed-load formulas of Camenen and Larson (2005) to ensure repeatability of the experiments. A transport equation is proposed for noncohesive sediments in steady flows from a wide range of data

$$\langle \overline{q_{sb}} \rangle = \rho_s \sqrt{\left(\frac{\rho_s}{\rho} - 1\right) gD_{50} 3\alpha \bar{\theta}^{\beta}} e^{\left(-\gamma \frac{\theta_c}{\bar{\theta}}\right)} \tag{6}$$

where the critical value of shear stress for grain motion θ_c is set here to 0.02 (based on preliminary experiments), the freshwater density ρ is 1,000 kg m^{-3}, and the empirical coefficients are $\alpha = 12$, $\beta = 1.5$, and $\gamma = 4.5$. Eq. (6) is compared to the estimated bed load to determine the accuracy of the CT scan method. The coefficient of determination (R^2) is estimated for CT and sand trap methods by using

$$R^2 = 1 - \frac{\sum (\overline{q_{sbi}} - f_i)^2}{\sum (\overline{q_{sbi}} - \overline{q_{sbmean}})^2} \tag{7}$$

where f is the function of Eq. (6) fitted to the data. The summation of Eq. (7) is calculated over the number of elements i that corresponds to the number of measurements. The coefficient R^2 is used to determine the precision of measurements, where a value close to 1 indicates a great precision.

Experimental Setup

An acrylic flume 0.30 m × 0.30 m × 7.0 m with 0.025-m-thick walls was inserted longitudinally and horizontally (no slope) into the medical CT scanner of the Multidisciplinary Laboratory for Non-Medical Use at the Institut National de la Recherche Scientifique (INRS, Québec) [Fig. 1(a)]. This scanner (Siemens, Somatom Definition AS+ 128) moves on 2.6-m rails along the flume in the longitudinal x-axis. A series of four experiments (EXP1 to EXP4) is performed at different initial water depth over a flat bed (d),

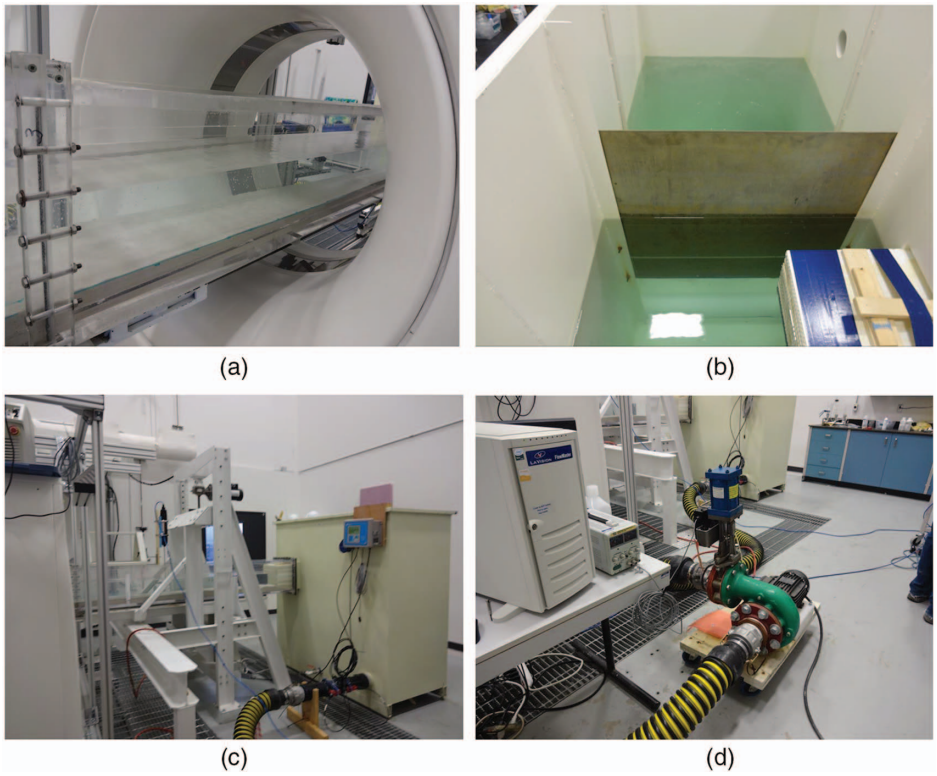

Fig. 1. (Color) Experimental setup components: (a) the rectangular hydraulic flume inserted into the medical X-ray CT scanner; (b) inside view of the water tank, the honeycomb diffuser is on the bottom right; (c) the water tank downstream where the flume is inserted at the top left of the tank, the water outcomes at the bottom right, and the flow meter is attached to the top right corner of the tank (in blue); and (d) the water pump joins the two water tanks, upstream and downstream.

J. Hydraul. Eng., 2022, 148(12): 06022017

Downloaded from ascelibrary.org by INRAE on 12/06/22. Copyright ASCE. For personal use only; all rights reserved.

which is measured by the CT scanner, with increasing flow speed. Transitional to turbulent flows are induced by a water pump [Fig. 1(d)] joining two large water tanks (4 m^3) placed at each extremity of the flume [Figs. 1(b and c)]. The water level into the tanks is a continuity of the flume surface waters. A honeycomb diffuser reduces the turbulence at the water inlet [Fig. 1(b)]. The unidirectional flow is maintained for approximately 30 min until the mean ripple height becomes constant prior to CT scan measurements. Based on the model proposed by Soulsby et al. (2012), we verified that bed forms reached their equilibrium properties before 30 min.

The horizontal sand bed consists of pure (99%) quartz (SiO_2) sand grain with a density of $\rho_s = 2{,}650\ kg\,m^{-3}$, a median grain diameter D_{50} of 216 μm, and a 90th percentile D_{90} of 355 μm. The sand bed is flattened manually before each experiment to obtain an initial bed thickness of 0.05 m. Table 1 summarizes the experimental conditions. A plexiglass box is placed at the downstream end of the flume where the sand in the bed-load layer can fall in. The bed-load rate per unit width ($kg\,m^{-2}$) is computed by weighing the dried sediments of the trap for a similar series of discharges (Camenen et al. 2017).

CT Scan Data Acquisition

The initial measurements are 360-degree 1D X-ray projections through the cross-section of the flume. The 3D matrix is reconstructed with a weighted filtered back-projection (Stierstorfer et al. 2004). For the experiments, the X-ray beam collimation is 1.2 mm, and the X-ray tube current intensity was 287 m with a tube voltage of 140 kV. The pitch factor, determining the gantry velocity during measurements in spiral mode (see below), is set to 0.35. The convolution kernel used to remove noise in the image reconstruction is a soft image smoothing Siemens filter (B30s). The CT measurement results in a 3D HU matrix of 512×512 pixels with a resolution of 0.6 mm in the cross-section (zy) and 2.0 mm in the longitudinal axis (x). Each scan is acquired within seconds. Two consecutive CT scans of a given length (L), separated by a time interval (T), are used to detect the 2D movement of sand ripples in the plane xy. As the bed-form velocity increases, the length of the scan (L) needs to be shortened to reduce the time T between two consecutive scans (see Table 1). The time T between two scans is directly limited by the cooling time required by the CT scanner. For EXP1, EXP2, and EXP3, the scans are acquired in the spiral mode where the CT scanner moves on the rails, allowing a long scans and sufficiently long time T to track the displacement of bed forms. For EXP4, where the bed-form velocity is the highest, the scan is performed in the static mode and the scanner does not move. This allows shorter time T than the spiral mode but with shorter length L. Nevertheless, L remains long enough to allow measurements covering at least the equivalent of one bed-form wavelength (i.e., crest-to-crest of bed structures), as the bed migrates within the flume.

CT Image Postprocessing

One of the main CT artifacts affecting this study is beam hardening (Ketcham and Hanna 2014). It refers to the preferential attenuation of the low-energy photons of the X-ray source, which tends to underestimate the HU values at the center of objects (Brooks and Di Chiro 1976). In this study, an empirical correction is applied to CT scan cross-section images of the flume to reduce the beam hardening artifacts, as proposed by Brunelle et al. (2015). In short, HU values given by a correction matrix (M_{cor}), calculated following Eqs. (8*a*)–(8*c*), are subtracted from the original CT scan image, as shown in Fig. 2

$$\phi(y,z) = a\tan\left(\frac{Y(y,z)}{Z(y,z)}\right) \tag{8a}$$

$$r(y,z) = \sqrt{Y^2(y,z) + Z^2(y,z)} \tag{8b}$$

$$M_{cor}(y,z) = (0.08r^2(y,z)|\cos(2\varphi(y,z))|^2) - 100 \tag{8c}$$

where $Y(y,z)$ and $Z(y,z)$ are the matrix of position index for each pixel centered in the middle of CT scan image.

Results

The three terms of Eq. (1) and bed-load transport have been obtained as follows. The dry sand bed density ρ_{sb} is first estimated using Eq. (2) and the HU values. The CT scan images in the cross-section of the flume [Fig. 2(a)] shows a range of HU values, indicating some ρ_{sb} variations within the bed. This variation is interpreted as the measurement error of ρ_{sb}. To reduce this error, mainly caused

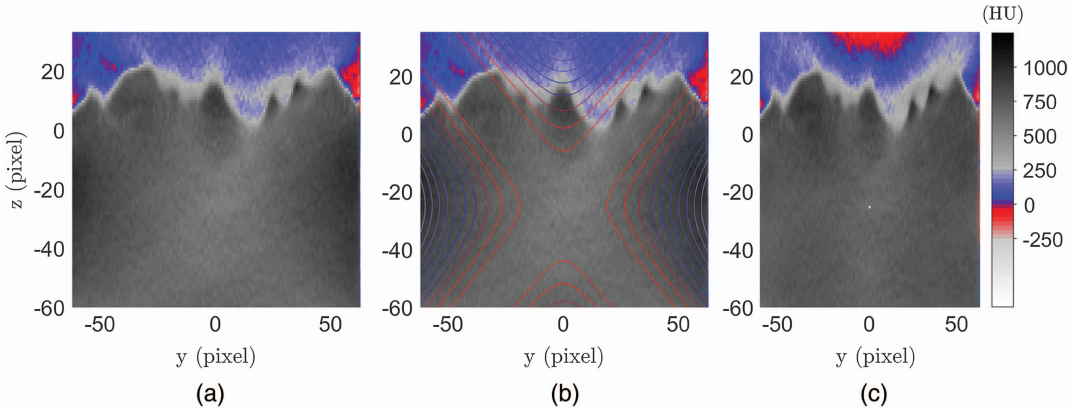

Fig. 2. (Color) Illustration for EXP4 of (a) raw HU values in the flume cross-section; (b) raw HU value in the background and correction in colored contour plot; and (c) corrected HU values. The colored contours indicate the HU value subtracted. The minimum value is –100 HU (red) and the maximum value is 250 HU (blue). The distribution of the correction is chosen to preserve the same HU spatial mean before and after the correction.

J. Hydraul. Eng., 2022, 148(12): 06022017

Downloaded from ascelibrary.org by INRAE on 12/06/22. Copyright ASCE. For personal use only; all rights reserved.

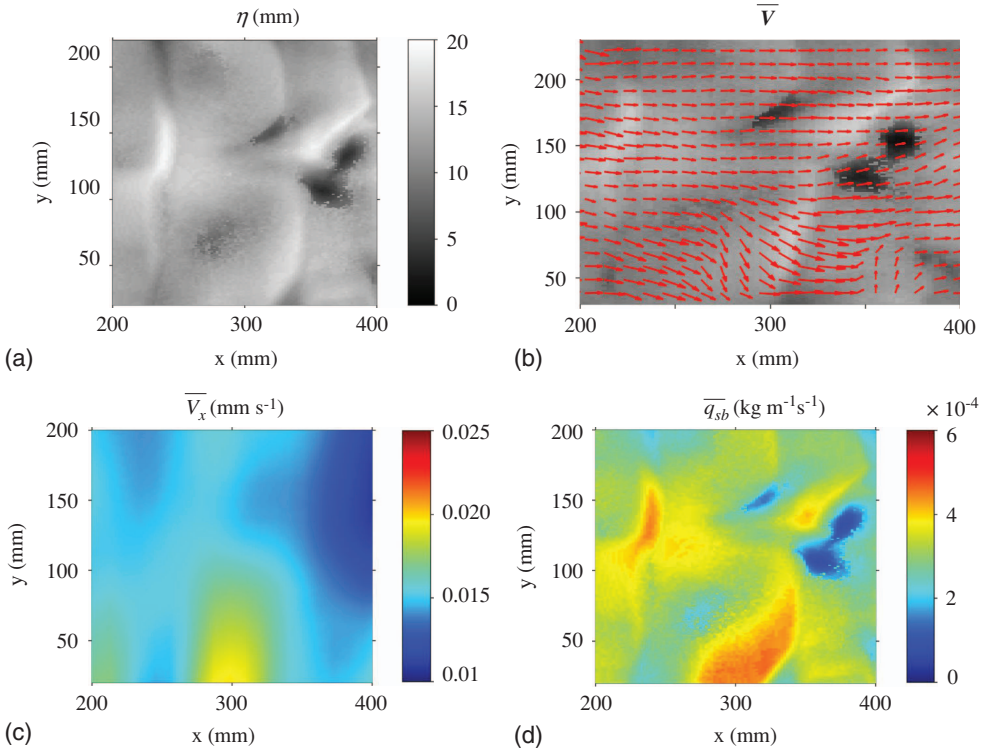

Fig. 3. (Color) Illustration for EXP1 of (a) bed elevation; (b) time-averaged velocity vector field of bed forms; (c) bed-form time-averaged velocity in the flow direction (x-axis); and (d) spatial distribution of time-averaged bed-load transport.

by the beam hardening artifact, a correction [Eqs. (8*a*)–(8*c*)] is applied [Fig. 2(b)] to CT scan images. The result is illustrated in Fig. 2(c), which shows that most of the beam hardening artifacts within the bed are removed. However, the correction does a poor job in the bed-load layer (i.e., at the water sediment interface). The remaining error for ρ_{sb} is estimated by calculating the standard deviation of the 3D spatial distribution of $\rho_{sb}(x, y, z)$. The 3D spatial mean of sand bed density $<\rho_{sb}(x, y, z)>_{xyz}$ and errors are listed in Table 1 for each experiment. The second term of Eq. (1) is estimated from the bed-form velocity vector field ($\bar{V}(x, y)$) [Fig. 3(b)]. Only the time-averaged bed-form velocity in the streamwise direction $\bar{V}_x(x, y)$ [Fig. 3(c)] is used to calculate the spatial distribution of bed load [Fig. 3(d)]. The third term of Eq. (1), the bed elevation, is illustrated in Fig. 3(a) neglecting the change in time of bed forms. The spatial distribution of the time-averaged bed load $\bar{q}_{sb}(x, y)$ is then computed as illustrated in Fig. 3(d).

The spatial means of bed load $<\bar{q}_{sb}(x, y)>_{xy}$ are listed in Table 1 for each experiment. $<\bar{q}_{sb}(x, y)>_{xy}$ is plotted as a function of $\bar{\theta}$ in Fig. 4. The error for bed elevation $\eta(x, y)$ and bed-form velocity measurements, estimated as 1% and 10%, respectively, are propagated additionally to the error for $<\rho_{sb}(x, y, z)>_{xyz}$ [Eq. (1*b*)] to estimate the error on the bed load. The error is on average 17.5 % for the sand bed density, according to the standard deviation of $\rho_{sb}(x, y, z)$. The error on bed load is thus estimated on average to be 20%. The uncertainty in $\bar{\theta}$ computation ($\pm$10%) mainly comes from the water discharge measurements that are used to estimate $\bar{U}$ [Eqs. (3) and (5)].

These results indicate that the precision of the bed load is low. However, $<\bar{q}_{sb}(x, y)>_{xy}$ values are accurate according to the sand traps. Indeed, the sand trap measurements, equivalent to term $<\bar{q}_{sb}(x, y)>_{xy}$, are in satisfactory agreement with the CT scan measurements (Fig. 4). The accuracy of the new method compared to trap values even improves for higher sediment transport rates.

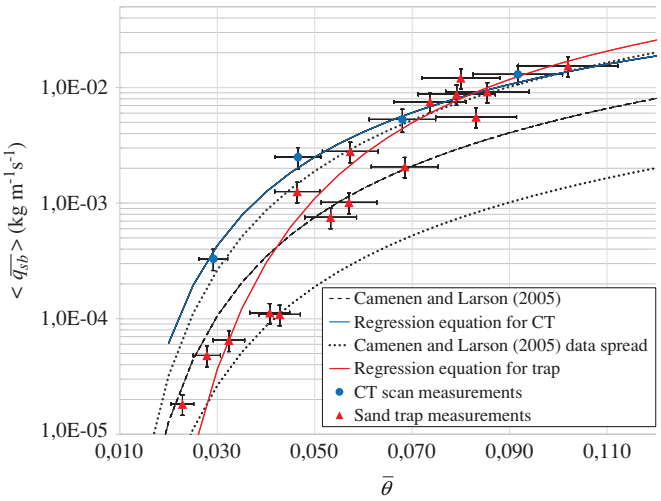

Fig. 4. (Color) Comparison of time- and spatial-averaged bed-load transport [$<\bar{q}sb(x, y) > xy$] calculated with CT scan and sand trap as a function of the time-averaged Shield parameter $\bar{\theta}$ for each experiment (EXP1–4). Previous results of literature are shown. The regression between $<\bar{q}sb(x, y) > xy$ and $\bar{\theta}$ is calculated by fitting the data to the Camenen and Larson (2005) equation for the sand trap ($\alpha = 13$, $\beta = 0.4$, $\gamma = -12$) and CT scan ($\alpha = 12$, $\beta = 1.1$, $\gamma = -4.5$).

All the CT scan data are also within an acceptable range compared to the bed-load equation of Camenen and Larson (2005). Moreover, $<\bar{q}_{sb}(x, y)>_{xy}$ values estimated with the CT method have a higher coefficient of determination [Eq. (7)], with $\bar{\theta}$ ($R^2 = 0.94$) when

Downloaded from ascelibrary.org by INRAE on 12/06/22. Copyright ASCE. For personal use only; all rights reserved.

fitting the data using the Camenen and Larson (2005) equation [Eq. (6)], than the sand traps ($R^2 = 0.11$).

Discussion and Conclusion

The experiments showed that the CT scan method accurately calculates the bed-load transport by correctly estimating the average sand bed density. However, the method deals with severe CT scan image artifacts, which are the main cause of error for sand bed density measurements and consequently, for bed-load transport calculation. Medical CT scanners have not been optimized for thick and dense objects with sharp edges such as a sand bed in a flume, but for the human body, which has a density closer to water. These errors are caused by the density, thickness, and sharp edges of the sand bed, which are unusual for a medical CT. While the correction proposed for CT scan image postprocessing performed well within the sand bed, it was less efficient for the bed-load layer where irregular ripples formed. The weighted filtered back-projection image reconstruction algorithm provided by the CT scanner manufacturer produced artifacts on these asymmetrical bed forms in the cross-section. Advanced beam hardening reduction, such as iterative image reconstruction algorithms, could help in reducing these kinds of artifacts but are numerically intense and require knowledge of the scanner geometry (Di Schiavi Trotta et al. 2022); however, they are viable options to improve image quality.

The experimental setup is also limited to the CT scan system capacity. The size, mainly the thickness, of the sand beds is limited, because beds thicker than 0.05 m would attenuate the X-rays to a point that could cause an unmanageable signal-to-noise ratio. The CT scan method is, moreover, limited by the cooling time needed by the X-ray system. This means that the time between two successive scans cannot be shorter than 30 s, limiting the length of the topography to 0.1 m. During the experiments, it was also determined that the maximum velocity of bed forms that can be detected using this configuration is around 0.6 mm s^{-1}. Long scans (i.e., up to 2 m) can be used to detect the movement of ripples if the velocity is not higher than 0.016 mm s^{-1}.

The advantage of the CT scan method over the sand traps is the capacity to provide spatial and temporal variations of bed-load transport, including the sand bed density measurements. The correlation between bed-load data with the bed-shear stress is higher for CT scans than for sand traps. This highlights the benefit of mass flux calculation with the bed-forms tracking method. The sand trap methods are likely to induce error from sand manipulation. The proposed CT scan method could be applicable to any future bed-load transport experiment studying the link between sediment density and bed dynamics within the limitations discussed above. This work can be conducted in parallel with the micro-CT scan imaging technique, which could determine physical properties of sediments at higher resolution using smaller samples (Mayar et al. 2020; Hodge et al. 2020). This work proved to deliver meaningful bed-load measurements for migrating ripples and is most promising for the study of symmetric wave ripples that would produce fewer image artifacts, or to the study of the sediment dynamics below the ripple zone, such as the infiltration of fine sediment into a coarse and porous sediment bed (Camenen et al. 2017).

Data Availability Statement

All data, models, or code generated or used during the study are available in a repository or online in accordance with funder data retention policies (Brunelle 2021).

Acknowledgments

This research was possible thanks to a CFI grant and a Research Chair in Coastal and fluvial engineering from the Ministère de la Sécurité publique et le Ministère des Transports of Québec Province, both awarded to Bernard Long. Corinne Brunelle also received support from Québec-Océan, a strategic cluster funded by FRQNT. This study was also partially supported by INRAE, as well as the Auvergne-Rhône-Alpes region through the CMIRA ExploraPro financial support (B. Camenen) and CMIRA Coopera financial support, and by a Canada Research Chair Tier1 in Environmental sedimentology awarded to PF. The authors would like to thank Pascal Bernatchez, Yves Secretan, Jan Franssen, and Bernard Long for fruitful discussions. The authors would also like to thank the two anonymous reviewers.

Notation

The following symbols are used in this paper:

HU = Hounsfield unit of CT scan;
q_{sb} = sand bed load rate per unit width (kgm^{-1}s^{-1});
U = water velocity (ms^{-1});
$\boldsymbol{V}$ = bed forms velocity vector (ms^{-1});
V_x = bed form velocity in the x direction (ms^{-1});
η = sand bed elevation (m);
θ = Shields' parameter;
ρ = water density (kgm^{-3});
ρ_s = sand grain density (kgm^{-3});
ρ_{sb} = dry sand bed density (kgm^{-3});
$<>_{x\cdot y\cdot z}$ = spatial mean in x, y, z-dimensions; and
$\bar{}$ = temporal mean.

References

Bevington, P. R., and D. K. Robinson. 2003. *Data reduction and error analysis*. 3rd ed. New York: McGraw-Hill.

Blanckaert, K., J. Heyman, and C. D. Rennie. 2017. "Measuring bedload sediment transport with an acoustic Doppler velocity profiler." *J. Hydraul. Eng.* 143 (6): 04017008. https://doi.org/10.1061/(ASCE)HY.1943-7900.0001293.

Brooks, R. A., and G. Di Chiro. 1976. "Beam hardening in X-ray reconstructive tomography." *Phys. Med. Biol.* 21 (3): 390. https://doi.org/10.1088/0031-9155/21/3/004.

Brunelle, C. 2019. "Apport de la tomodensitométrie à l'étude du transport sédimentaire." [In French.] Ph.D. thesis, Institut National de la Recherche Scientifique, Université du Québec.

Brunelle, C. 2021. "X-ray computed tomography to measure real-time porosity in bedload transport experiment." Accessed December 15, 2021. https://borealisdata.ca/dataset.xhtml?persistentId=doi:10.5683/SP2/SUNA2L#.

Brunelle, C., B. Long, P. Francus, L.-F. Daigle, M. Desroches, and H. Takayama. 2015. "Wave-sediment interaction imaging with X-ray tomography: A small-scale experiment to characterize the artefacts." In *Proc., 2nd Int. Conf. on Tomography of Materials and Structures*. Québec: Institut National de la Recherche Scientifique.

Camenen, B., and M. Larson. 2005. "A general formula for non-cohesive bed load sediment transport." *Estuaries Coastal Shelf Sci.* 63 (1–2): 249–260. https://doi.org/10.1016/j.ecss.2004.10.019.

Camenen, B., E. Perret, C. Brunelle, P. Francus, M. Des Roches, and L.-F. Daigle. 2017. "Dynamics of a fine and coarse sediment mixture using a medical CT scan." In *Proc., 10th RCEM Symp.* Trento, Italy: Univ. of Trento.

Di Schiavi Trotta, L., D. Matenine, M. Martini, K. Stierstorfer, Y. Lemaréchal, P. Francus, and P. Després. 2022. "Beam-hardening corrections through a polychromatic projection model integrated to an

Downloaded from ascelibrary.org by INRAE on 12/06/22. Copyright ASCE. For personal use only; all rights reserved.

iterative reconstruction algorithm." *NDT&E Int.* 126 (Mar): 102594. https://doi.org/10.1016/j.ndteint.2021.102594.

Griffin, L. D., P. Elangovan, A. Mundell, and D. C. Hezel. 2012. "Improved segmentation of meteorite micro-CT images using local histograms." *Comput. Geosci.* 39 (Feb): 129–134. https://doi.org/10.1016/j.cageo.2011.07.002.

Hodge, R. A., H. Voepel, J. Leyland, D. A. Sear, and S. Ahmed. 2020. "X-ray computed tomography reveals that grain protrusion controls critical shear stress for entrainment of fluvial gravels." *Geology* 48 (2): 149–153. https://doi.org/10.1130/G46883.1.

Holmes, R. R., Jr. 2010. *Measurement of bedload transport in sand-bed rivers: A look at two indirect sampling methods*. US Geological Survey Scientific Investigations Rep. 5091. Reston, VA: USGS.

Hsieh, J. 2009. *Computed tomography: Principles, design, artifacts, and recent advances*. Bellingham, WA: SPIE Press.

Hurther, D., P. D. Thorne, M. Bricault, U. Lemmin, and J. M. Barnoud. 2011. "A multi-frequency acoustic concentration and velocity profiler (ACVP) for boundary layer measurements of fine-scale flow and sediment transport processes." *Coastal Eng.* 58 (7): 594–605. https://doi.org/10.1016/j.coastaleng.2011.01.006.

Kastengren, A., and C. F. Powell. 2014. "Synchrotron X-ray techniques for fluid dynamics." *Exp. Fluids* 55 (3): 1686. https://doi.org/10.1007/s00348-014-1686-8.

Ketcham, R. A., and W. D. Carlson. 2001. "Acquisition, optimization and interpretation of X-ray computed tomographic imagery: Applications to the geosciences." *Comput. Geosci.* 27 (4): 381–400. https://doi.org/10.1016/S0098-3004(00)00116-3.

Ketcham, R. A., and R. D. Hanna. 2014. "Beam hardening correction for X-ray computed tomography of heterogeneous natural materials." *Comput. Geosci.* 67 (Jun): 49–61. https://doi.org/10.1016/j.cageo.2014.03.003.

Ketcham, R. A., and G. J. Iturrino. 2005. "Nondestructive high-resolution visualization and measurement of anisotropic effective porosity in complex lithologies using high-resolution X-ray computed tomography." *J. Hydrol.* 302 (1–4): 92–106. https://doi.org/10.1016/j.jhydrol.2004.06.037.

Khorram, S., and M. Ergil. 2011. "Determining the predominant governing parameters of the bed-load equations for sediment-laden rivers on the continental shelf." *J. Coastal Res.* 27 (2): 276–290. https://doi.org/10.2112/JCOASTRES-D-09-00127.1.

Khosravi, K., A. H. Chegini, A. D. Binns, P. Daggupati, and L. Mao. 2019. "Difference in the bed load transport of graded and uniform sediments during floods: An experimental investigation." *Hydrol. Res.* 50 (6): 1645–1664. https://doi.org/10.2166/nh.2019.078.

Mayar, M. A., G. Schmid, S. Wieprecht, and M. Noack. 2020. "Proof-of-concept for nonintrusive and undisturbed measurement of sediment infiltration masses using gamma-ray attenuation." *J. Hydraul. Eng.* 146 (5): 04020032. https://doi.org/10.1061/(ASCE)HY.1943-7900.0001734.

McElroy, B., and D. Mohrig. 2009. "Nature of deformation of sandy bed forms." *J. Geophys. Res. Earth Surf.* 114 (F3): F00A04. https://doi.org/10.1029/2008JF001220.

Mrokowska, M. M., P. M. Rowiński, L. Książek, A. Strużyński, M. Wyrębek, and A. Radecki-Pawlik. 2018. "Laboratory studies on bedload transport under unsteady flow conditions." *J. Hydrol. Hydromech.* 66 (1): 23–31. https://doi.org/10.1515/johh-2017-0032.

Muste, M., S. Baranya, R. Tsubaki, D. Kim, H. Ho, H. Tsai, and D. Law. 2016. "Acoustic mapping velocimetry." *Water Resour. Res.* 52 (5): 4132–4150. https://doi.org/10.1002/2015WR018354.

Nikuradse, J. 1933. "Strömungsgesetze in rauhen rohren forschhft." *Ver. Dt. Ing.* 36 (10): 1–62.

Otani, J., and Y. Obara. 2004. "X-ray CT for geomaterials: Soils, concrete, rocks." In *Proc., Int. Workshop on X-ray CT for Geomaterials*. Amsterdam, Netherlands: A.A. Balkema.

Roberts, J. D., R. A. Jepsen, and S. C. James. 2003. "Measurements of sediment erosion and transport with the adjustable shear stress erosion and transport flume." *J. Hydraul. Eng.* 129 (11): 862–871. https://doi.org/10.1061/(ASCE)0733-9429(2003)129:11(862).

Scarano, F. 2012. "Tomographic PIV: Principles and practice." *Meas. Sci. Technol.* 24 (1): 012001. https://doi.org/10.1088/0957-0233/24/1/012001.

Shields, A. 1936. "Anwendung der Aehnlichkeitsmechanik und der Turbulenzforschung auf die Geschiebebewegung." [In German.] Ph.D. thesis, Wasserbau und Schiffbau, Technical Univ. Berlin.

Soulsby, R. 1983. "The bottom boundary layer of shelf seas." In Vol. 35 of *Elsevier oceanography series*, 189–266. Amsterdam, Netherlands: Elsevier. https://doi.org/10.1016/S0422-9894(08)70503-8.

Soulsby, R., R. J. S. Whitehouse, and K. V. Marten. 2012. "Prediction of time-evolving sand ripples in shelf seas." *Cont. Shelf Res.* 38 (Apr): 47–62. https://doi.org/10.1016/j.csr.2012.02.016.

Stierstorfer, K., A. Rauscher, J. Boese, H. Bruder, S. Schaller, and T. Flohr. 2004. "Weighted FBP—A simple approximate 3D FBP algorithm for multislice spiral CT with good dose usage for arbitrary pitch." *Phys. Med. Biol.* 49 (11): 2209. https://doi.org/10.1088/0031-9155/49/11/007.

Tilston, M., R. Arnott, C. Rennie, and B. Long. 2015. "The influence of grain size on the velocity and sediment concentration profiles and depositional record of turbidity currents." *Geology* 43 (9): 839–842. https://doi.org/10.1130/G37069.1.

Tsubaki, R., S. Baranya, M. Muste, and Y. Toda. 2018. "Spatio-temporal patterns of sediment particle movement on 2D and 3D bedforms." *Exp. Fluids* 59 (6): 93. https://doi.org/10.1007/s00348-018-2551-y.

Yalin, M. S. 1972. *Mechanics of sediment transport*, 298. Oxford, UK: Pergamon Press.

Yamada, F., R. Tateyama, G. Tsujimoto, S. Suenaga, B. Long, and C. Pilote. 2013. "Dynamic monitoring of physical models beach morphodynamics and sediment transport using X-ray CT scanning technique." Supplement, *J. Coastal Res.* 165 (S2): 1617–1622. https://doi.org/10.2112/SI65-273.1.

Downloaded from ascelibrary.org by INRAE on 12/06/22. Copyright ASCE. For personal use only; all rights reserved.